### Title

Reentrant Structural and Optical Properties and Large Positive Thermal Expansion in Perovskite Formamidinium Lead Iodide




### Journal

Angewandte Chemie International Edition, 55(49)

### ISSN

14337851



### Authors

Fabini, Douglas H
Stoumpos, Constantinos C
Laurita, Geneva
et al.



### Publication Date

2016-12-05

### DOI

10.1002/anie.201609538

Peer reviewed

# Reentrant Structural and Optical Properties and Large Positive Thermal Expansion in Perovskite Formamidinium Lead Iodide

Douglas H. Fabini,[a,b] Constantinos C. Stoumpos,[c] Geneva Laurita,[a] Andreas Kaltzoglou,[d] Athanassios G. Kontos,[d] Polycarpos Falaras,[d] Mercouri G. Kanatzidis,[c] and Ram Seshadri*[a,b,e]

**Abstract:** The structure of the hybrid perovskite $HC(NH_2)_2PbI_3$ (formamidinium lead iodide) reflects competing interactions associated with molecular motion, hydrogen bonding tendencies, thermally activated soft octahedral rotations, and the propensity for the $Pb^{2+}$ lone pair to express its stereochemistry. High-resolution synchrotron X-ray powder diffraction reveals a continuous transition from the cubic α-phase ($Pm\bar{3}m$, #221) to a tetragonal β-phase ($P4/mbm$, #127) at around 285 K, followed by a first-order transition to a tetragonal γ-phase (retaining $P4/mbm$, #127) at 140 K. An unusual reentrant pseudosymmetry in the β–to–γ phase transition is seen that is also reflected in the photoluminescence. Around room temperature, the coefficient of volumetric thermal expansion is among the largest for any extended crystalline solid.

Photovoltaic absorbers based on the hybrid perovskite $HC(NH_2)_2PbI_3$ (formamidinium lead iodide) and its alloys exhibit impressive performance,[1] but the description of the crystal structure of this material is incomplete. In addition to this technological motivation,[2] dense hybrid materials with 3-D inorganic connectivity and isolated organic molecular ions combine features of traditional inorganic solids and open framework materials, and their composition–structure relations are of fundamental interest.

The initial report of the preparation and characterization of $HC(NH_2)_2PbI_3$ proposed perovskite structures of trigonal symmetry for the α- and β-phases on the basis of laboratory single crystal X-ray diffraction,[3] while a subsequent report assigned the structure of the cubic perovskite aristotype for the α-phase from neutron powder diffraction.[4] The structure of the γ-phase has not been reported.

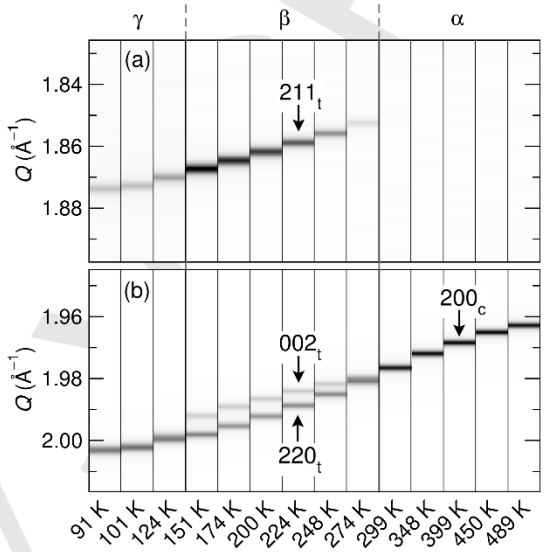


**Figure 1.** X-ray scattering intensity from $HC(NH_2)_2PbI_3$ around selected low-angle Bragg peaks between 90 K and 490 K, normalized to maximum peak intensity. (a) The $211_t$ tetragonal Bragg peak emerges upon cooling through a continuous phase transition around 285 K from the cubic α-phase to the tetragonal β-phase. (b) The $200_c$ cubic Bragg peak splits continuously on cooling due to the emergent tetragonality. A first order transition to the pseudo-cubic γ-phase with tetragonal symmetry occurs at 140 K.[5] The $002_t$ and $220_t$ tetragonal peaks "fuse" across the β–γ transition while the $211_t$ tetragonal peak remains.

The disordered molecular cation, challenges associated with twinning in single crystals, and issues of pseudosymmetry led us to employ high-resolution synchrotron X-ray powder diffraction to follow the structure evolution of $HC(NH_2)_2PbI_3$ between 90 K and 490 K. The temperature-dependent scattering intensity around instructive low-angle Bragg peaks is given in Figure 1. The continuous α–β phase transition around 285 K is evident in the emergence of the 211 tetragonal peak and the splitting of the 200 cubic peak into the 002 and 220 tetragonal peaks on cooling. The first-order β–γ transition can be seen in the abrupt change in intensities and peak positions at 140 K (transition temperature from reported scanning calorimetry, which confirms the order of the transitions[5]). Remarkably, the 002 and 220 tetragonal peaks "fuse" in the γ-phase, while the 211 tetragonal peak remains, suggesting the possibility of a tetragonal phase with cubic pseudosymmetry.

Le Bail and Rietveld analyses of diffraction data confirm this hypothesis. In agreement with the results of Weller et al.,[4] the α-phase is well described by the cubic $Pm\bar{3}m$ aristotype ($a$ = 6.35788 Å at 299 K), as shown in Figure 2(a). For all phases, the $A$-site $[HC(NH_2)_2]^+$ cation has been modeled as a pseudo-atom with equivalent scattering power due to the dynamic disorder (*vide infra*) and limited sensitivity in the X-ray experiment.

[a] D. H. Fabini, Dr. G. Laurita, Prof. Dr. R. Seshadri
Materials Research Laboratory, University of California
Santa Barbara, CA 93106 (USA)
E-mail: seshadri@mrl.ucsb.edu
[b] D. H. Fabini, Prof. Dr. R. Seshadri
Materials Department, University of California
Santa Barbara, CA 93106 (USA)
[c] Dr. C. C. Stoumpos, Prof. Dr. M. G. Kanatzidis
Chemistry Department, Northwestern University
Evanston, IL 60208 (USA)
[d] Dr. A. Kaltzoglou, Dr. A. G. Kontos, Dr. P. Falaras
Institute of Nanoscience and Nanotechnology, NCSR Demokritos
Athens 15310, Greece
[e] Prof. Dr. R. Seshadri
Department of Chemistry and Biochemistry, University of California
Santa Barbara, CA 93106 (USA)

Supporting information for this article is given via a link at the end of the document.

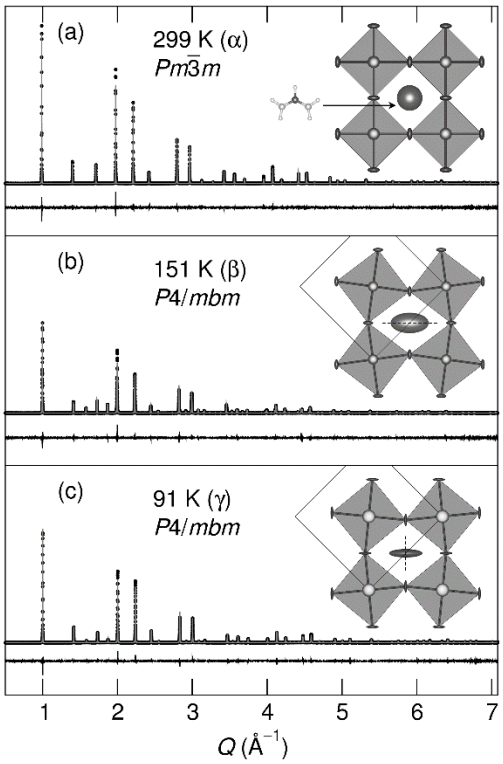


**Figure 2.** Rietveld refinement of X-ray powder diffraction and resulting crystal structures of the phases of $HC(NH_2)_2PbI_3$. Recorded scattering intensities are indicated by black dots, modelled intensities by grey lines, and difference curves are offset below. The *A*-site $[HC(NH_2)_2]^+$ cation is modelled as a pseudo-atom with the same form factor due to disorder and limited sensitivity in the X-ray experiment, and atomic displacement parameter (ADP) ellipsoids are visualized at the 50% level. (a) Cubic α-phase (*Pm*$\bar{3}$*m*, #221) at 299 K, $R_w$ = 12.4%. The formamidinium cation, $[HC(NH_2)_2]^+$ is illustrated. (b) Tetragonal β-phase (*P*4/*mbm*, #127) at 151 K, $R_w$ = 15.1%, viewed down the c-axis. (c) Tetragonal γ-phase (*P*4/*mbm*, #127) at 91 K, $R_w$ = 16.1%, viewed down the c-axis. Dashed lines in (b,c) indicate the unique axis of the *A*-site ADP ellipsoid.

The structure of the β-phase is that of *P*4/*mbm* symmetry, with $a^0a^0c^+$ tilts in Glazer notation[6] (temperature-dependent structure parameters for all phases are provided in the Supporting Information). This in-phase uniaxial tilt pattern (Figure 2(b)) is in line with computational predictions of the preferred tilts for tetragonal perovskite iodides[7] and contrasts with the out-of-phase tilts observed in the tetragonal phase of $CH_3NH_3PbI_3$[8] and many oxides. The anisotropy of the *A*-site atomic displacement parameters (ADPs) suggests preferential orientations for the molecular cation due to the tilting of the octahedra.

Remarkably, the structure of the γ-phase is also that of $a^0a^0c^+$ tilts with *P*4/*mbm* symmetry, as shown in Figure 2(c), though there are discontinuous changes in many structure parameters (*vide infra*) as required for such a first-order transition. Alternative structures exhibiting simple tilts that maintain 3-D octahedral connectivity[9] and that allow ferroic $Pb^{2+}$ displacements[10] were screened and rejected based on unindexed peaks, absences of expected peaks, or both (details given in the Supporting Information).

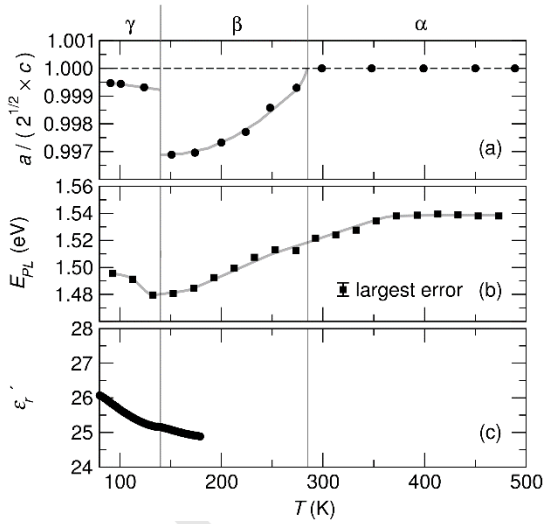


**Figure 3.** Tetragonal lattice parameter ratio, photoluminescence peak energy, and static dielectric permittivity of $HC(NH_2)_2PbI_3$. (a) The tetragonal lattice parameter ratio reflects the continuous α–β transition on cooling, as well as the reentrant cubic pseudosymmetry in the γ-phase. Error bars are smaller than the markers and are omitted. (b) The photoluminescence (PL) emission peak energy, $E_{PL}$, red-shifts on warming through the γ–β transition. In the β- and α-phases, $E_{PL}$ blue-shifts with temperature, consistent with the effects of lattice expansion[11] on the unusual electronic structure of the main-group halide perovskites, and subsequently plateaus above 370 K. (c) Static dielectric permittivity, $\varepsilon_r$', extracted from capacitance–loss measurements at 20 kHz. Despite a slight kink at the β–γ transition, $\varepsilon_r$' declines substantially with temperature in both phases, suggesting reorientation of the dipolar axis of the *A*-site cation is minimally inhibited even at these temperatures.

Given this highly unusual phase evolution, we examined the temperature dependence of structure parameters from Rietveld refinement of diffraction data across the temperature range of 90 K to 490 K, as well as temperature-dependent optical and dielectric properties. The tetragonal lattice parameter ratio is given in Figure 3(a), and reflects the continuous emergence of tetragonality on cooling into the β-phase, as well as the reentrant cubic pseudosymmetry in the γ-phase.

The photoluminescence (PL) emission peak energy, $E_{PL}$, is given in Figure 3(b). $E_{PL}$ blue-shifts with temperature in the α- and β-phases, consistent with the effects of thermal expansion on the unusual electronic structure as well as possible dynamic $Pb^{2+}$ displacements.[11] $E_{PL}$ plateaus above 370 K, a range which was not accessed in previous studies. On cooling through the β–γ transition, $E_{PL}$ blue-shifts substantially, in agreement with existing reports.[12,13] This is similar to the observed behavior at the tetragonal–orthorhombic transition in $CH_3NH_3PbI_3$,[13] where the blue-shift arises from reduced Pb–I orbital overlap due to the lowered symmetry, though in $HC(NH_2)_2PbI_3$ the blue-shift despite reduced tilting suggests crystallographically hidden disorder of the Pb–I network, though no disorder-induced emission broadening is apparent.

The static dielectric permittivity, $\varepsilon_r$', indirectly probes the rotational freedom of the polar axis of the molecular cation.[14] For the well-studied $CH_3NH_3PbI_3$, $\varepsilon_r$' rises on cooling in the tetragonal phase and drops abruptly through the tetragonal–orthorhombic phase transition,[15] as the severe tilting of the octahedra constrains the reorientation of the C–N axis. In contrast, $\varepsilon_r$' for

$HC(NH_2)_2PbI_3$ has no discontinuity and continues to rise on cooling in the γ-phase (Figure 3(c)), suggesting minimally inhibited reorientation of the polar axis. The smaller value and reduced temperature dependence of $\varepsilon_r$' compared to that for $CH_3NH_3PbI_3$ are consistent with the smaller dipole moment for $[HC(NH_2)_2]^+$. The persistence of considerable cation motion in the γ-phase is in line with our previous observation of a glassy slowing of dynamics below 100 K in $CH_3NH_3PbI_3$ and $HC(NH_2)_2PbI_3$, with $HC(NH_2)_2PbI_3$ exhibiting greater glass fragility.[5]

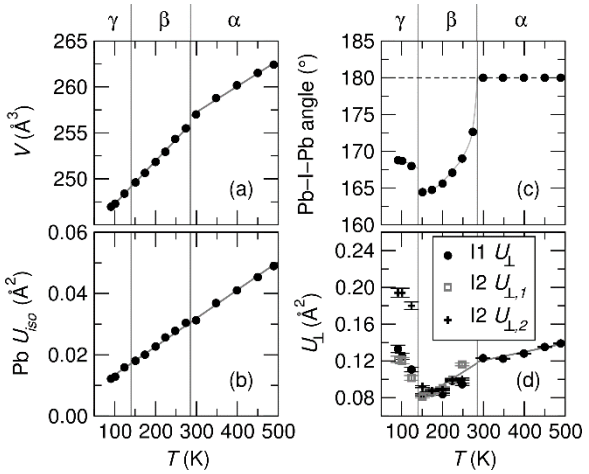


**Figure 4.** Selected crystallographic parameters for $HC(NH_2)_2PbI_3$. Error bars for (a)–(c) are smaller than the markers and are omitted. (a) The unit cell volume per formula unit, *V*, reveals unusually large volumetric thermal expansion coefficients ($\alpha_V$ = 203 × $10^{-6}$ $K^{-1}$ at 274 K). $\alpha_V$ is reduced in the cubic phase, consistent with a negative contribution from large amplitude dynamic octahedral tilts.[16-18] (b) The isotropic ADP for Pb, $U_{iso}$, is large compared to typical values in oxides but reveals no discontinuities associated with masked displacements in the tetragonal phases. (c) The Pb–I–Pb octahedral tilt angle reflects the continuous α–β transition, and jumps back toward linear through the unusual β–γ transition. (d) The ADPs for I in the directions orthogonal to the Pb–I bonds, $U_\perp$, decline monotonically with cooling in the α- and β-phases, consistent with reduced dynamic octahedral tilting. The increased values of the $U_\perp$ ADPs on cooling to the γ-phase suggest disorder that is not fully captured by this crystallographic model.

**Table 1.** Volumetric Thermal Expansion Coefficients, $\alpha_V$, of $HC(NH_2)_2PbI_3$ and Selected Other Compounds Near Room Temperature.

| Composition | Phase | *T* (K) | $\alpha_V$ ($10^{-6}$ $K^{-1}$) | Reference |
|---|---|---|---|---|
| $HC(NH_2)_2PbI_3$ | β (solid) | 200 – 299 | 206 – 202 | This work |
| $HC(NH_2)_2PbI_3$ | α (solid) | 348 – 489 | 100 – 98.6 | This work |
| $CH_3NH_3PbI_3$ | β (solid) | 280 | 132 | [19,20] |
| $CsSnI_3$ | γ (solid) | 298 | 126 | [21] |
| $Ag_3[Co(CN)_6]$ | Solid | 276 | 121 | [22] |
| Hg | Liquid | 293 | 182 | [21] |

The unit cell volume per formula unit, *V*, is given in Figure 4(a). A comparison of the volumetric thermal expansion coefficient, $\alpha_V$, with those of other main-group halides and selected framework materials and liquids is given in Table 1. Fit over a temperature range of 200 K to 299 K, $\alpha_V$ is greater than 200 × $10^{-6}$ $K^{-1}$ ($R^2$ = 99.8%). Thus, $\alpha_V$ for the β-phase is larger than that for liquid mercury[21] and appears to be nearly the largest for any extended crystalline solid near ambient temperature. It was recently reported that $\alpha_V$ = 220 × $10^{-6}$ $K^{-1}$ for the mixed *A*-site $[CH_3NH_3]_{0.5}[HC(NH_2)_2]_{0.5}PbI_3$, though the precise temperature and fitting range are unspecified.[23] In the β-phase, linear thermal expansion is ~60% greater in the ab-plane ($\alpha_a$ = 7.7 × $10^{-5}$ $K^{-1}$) than in the c-direction ($\alpha_c$ = 4.9 × $10^{-5}$ $K^{-1}$), suggesting anisotropic mechanical properties. While still large, $\alpha_V$ is substantially reduced in the cubic α-phase, consistent with a negative contribution from large amplitude dynamic octahedral tilts as in *A*-site vacant $ReO_3$[16,17] and $ScF_3$.[18]

The isotropic ADP for Pb, $U_{iso}$, is given in Figure 4(b), and increases monotonically with temperature. While the value is significantly elevated relative to typical values in oxides (partially a consequence of $6s^2$ lone pair-induced anharmonicity[11]), there are no discontinuities that would suggest crystallographic $Pb^{2+}$ displacements that are not captured in our structure models for the low temperature phases.

The Pb–I–Pb octahedral tilt angle is given in Figure 4(c), and reflects the continuous α–β transition. In the γ-phase, the tilt angle jumps closer to linear, underscoring the unusual nature of this transition.

Iodine ADPs in the directions orthogonal to the Pb–I bonds, $U_\perp$, are given in Figure 4(d). Consistent with thermally-activated dynamic octahedral tilts, the values of $U_\perp$ decrease monotonically on cooling in the α- and β-phases. However, they increase significantly in the γ-phase, again consistent with disorder that is not captured by this crystallographic model. The discrepancy between ADPs for the two distinct I sites in the γ-phase reflects parameter correlations that arise from Bragg peak overlap.

Together, the photoluminescence, iodine ADPs, and persistence of molecular motion in the γ-phase suggest complex (possibly modulated) disorder in this regime. This is supported by the observation of weak (intensity <0.5% that of the strongest Bragg peak) diffuse scattering features between *Q* = 1.55 $Å^{-1}$ and *Q* = 2.00 $Å^{-1}$ that are not indexed by any plausible space group symmetry.[9,10] Nonetheless, the pseudo-cubic unit cell is unambiguous, and underscores the different N–H···I interactions between $CH_3NH_3PbI_3$ and $HC(NH_2)_2PbI_3$, where the diamine may hydrogen bond to halogens on both sides of the cage.

In summary, we find that this class of materials, already so fascinating on account of their outstanding functionality in photovoltaic devices, display fundamental properties that are surprising and even counterintuitive. The implications for technological applications are profound. For example, the very large volumetric thermal expansion creates substantial challenges in device applications. The atomistic origins of the reentrant structural and optical behavior deserve further scrutiny.

## Experimental Section

$HC(NH_2)_2PbI_3$ was prepared following a modification of the previously reported procedure.[3] 4.46 g (20 mmol) of PbO was dissolved in 15 ml of concentrated aqueous HI (57% w/w) and the solution temperature was raised and held to boiling (ca. 130° C). In a separate beaker, 2.08 g (20 mmol) of $(HC(NH_2)_2)(O_2CCH_3)$ or 1.61 g (20 mmol) of freshly prepared $HC(NH_2)_2Cl$ (prepared from $(HC(NH_2)_2)(O_2CCH_3)$ and concentrated HCl (37% w/w), followed by copious washing with toluene to remove excess

acetic acid)[4] were dissolved in 5 mL of concentrated aqueous HI (57% w/w). The latter step was found to be necessary since commercially available $HC(NH_2)_2Cl$ is extremely hygroscopic and contains hydrolysis products. Addition of the $HC(NH_2)_2I$ solution to the $PbI_2$ solution resulted immediately in a fine black precipitate. The reaction was stopped after 5 min and the solution was filtered hot under vacuum to avoid co-precipitation of hydrated phases obtained for the cooled solution. During filtration, the black solid turns to yellow, completely converting over a period of 5 to 10 min. The yellow solid was transferred in a vacuum oven and heated at 120° C overnight, yielding a black solid that is stable for a period of 20 to 30 days before converting back to the yellow phase. Note that if the latter step is performed in an evacuated ampule under static vacuum, the black phase converts to the yellow one within 5 to 10 min. The obtained black material consists of the crystallographically pure α-phase of $HC(NH_2)_2PbI_3$. Yield: 9 to 10 g (70% to 80%).

High resolution synchrotron X-ray powder diffraction data were collected using beamline 11-BM at the Advanced Photon Source (APS), Argonne National Laboratory at a wavelength of 0.459200 Å. 50 mg of ground, yellow $HC(NH_2)_2PbI_3$ was packed and sealed into a 0.5 mm OD Kapton capillary. Complete conversion to the black perovskite phase was achieved in situ by heating initially to 490 K during data acquisition.

Candidate crystal structures for the phases of $HC(NH_2)_2PbI_3$ were generated using ISODISTORT (ISOTROPY Software Suite, iso.byu.edu). Le Bail and Rietveld analyses were performed using the GSAS software suite[24] with the EXPGUI interface.[25]

Photoluminescence measurements were performed on a Renishaw Invia spectrometer analyzing the backscattered filtered light emitted by a laser excitation at 785 nm. The samples were loaded into a THMS600PS Linkam optical cell under an inert Ar atmosphere. The incident beam was focused on spots of 5 $\mu m^2$. Power density was on the order of $\mu W\ \mu m^{-2}$, except above 433 K where the PL signal is very low and the incident power was raised to 0.12 $mW\ \mu m^{-2}$. PL spectra were recorded and averaged from five different spots at each temperature. The spectra from different spots have similar spectral characteristics but different absolute intensities, and spatial variation of peak position is only 1 to 2 nm.

A flat plate capacitor was prepared by grinding black $HC(NH_2)_2PbI_3$ and cold-pressing to 3 tons in a 6 mm diameter cylindrical die (pellet thickness 2.54 mm) and applying indium contacts via low temperature soldering. Capacitance–loss measurements were performed in a Quantum Design PPMS DynaCool using an Andeen-Hagerling AH 2700A Ultra-precision Capacitance Bridge over the frequency range 100 Hz to 20 kHz.

## Acknowledgements

This work was supported by the U.S. Department of Energy, Office of Science, Basic Energy Sciences under award number DE-SC-0012541. It is our pleasure to thank Professor Anthony K. Cheetham FRS for illuminating discussions. This research used resources of the Advanced Photon Source, a U.S. Department of Energy (DOE) Office of Science User Facility operated for the DOE Office of Science by Argonne National Laboratory under Contract No. DE-AC02-06CH11357. D.H.F. thanks the National Science Foundation Graduate Research Fellowship Program for support under Grant DGE 1144085. The MRL Shared Experimental Facilities are supported by the MRSEC Program of the NSF under Award No. DMR 1121053; a member of the NSF-funded Materials Research Facilities Network (www.mrfn.org). P.F. acknowledges financial support from FP7 European Union (Marie Curie ITN DESTINY/316494).

**Keywords:** perovskite phases • phase transitions • solid-state structures • thermal expansion • X-ray diffraction

[1] M. Saliba, T. Matsui, J.-Y. Seo, K. Domanski, J.-P. Correa-Baena, M. K. Nazeeruddin, S. M. Zakeeruddin, W. Tress, A. Abate, A. Hagfeldt, M. Grätzel, *Energy Environ. Sci.* **2016**, *9*, 1989–1997.

[2] B. V. Lotsch, *Angew. Chem., Int. Ed.* **2014**, *53*, 635–637.

[3] C. C. Stoumpos, C. D. Malliakas, M. G. Kanatzidis, *Inorg. Chem.* **2013**, *52*, 9019–9038.

[4] M. T. Weller, O. J. Weber, J. M. Frost, A. Walsh, *J. Phys. Chem. Lett.* **2015**, *6*, 3209–3212.

[5] D. H. Fabini, T. Hogan, H. A. Evans, C. C. Stoumpos, M. G. Kanatzidis, R. Seshadri, *J. Phys. Chem. Lett.* **2016**, *7*, 376–381.

[6] A. M. Glazer, *Acta Crystallogr. Sect. B* **1972**, *28*, 3384–3392.

[7] J. Young, J. M. Rondinelli, *J. Phys. Chem. Lett.* **2016**, *7*, 918–922.

[8] M. T. Weller, O. J. Weber, P. F. Henry, A. M. Di Pumpo, T. C. Hansen, *Chem. Commun.* **2015**, *51*, 4180–4183.

[9] C. J. Howard, H. T. Stokes, *Acta Crystallogr. Sect. B* **1998**, *54*, 782–789.

[10] H. T. Stokes, E. H. Kisi, D. M. Hatch, C. J. Howard, *Acta Crystallogr. Sect. B* **2002**, *58*, 934–938.

[11] D. H. Fabini, G. Laurita, J. S. Bechtel, C. C. Stoumpos, H. A. Evans, A. G. Kontos, Y. S. Raptis, P. Falaras, A. Van der Ven, M. G. Kanatzidis, R. Seshadri, *J. Am. Chem. Soc.* **2016**, *138*, 11820–11832.

[12] H.-H. Fang, F. Wang, S. Adjokatse, N. Zhao, J. Even, M. A. Loi, *Light Sci. Appl.* **2016**, *5*, e16056.

[13] A. D. Wright, C. Verdi, R. L. Milot, G. E. Eperon, M. A. Pérez-Osorio, H. J. Snaith, F. Giustino, M. B. Johnston, L. M. Herz, *Nat. Commun.* **2016**, *7*, 11755.

[14] W. Zhang, Y. Cai, R.-G. Xiong, H. Yoshikawa, K. Awaga, *Angew. Chem., Int. Ed.* **2010**, *49*, 6608–6610.

[15] N. Onoda-Yamamuro, T. Matsuo, H. Suga, *J. Phys. Chem. Solids* **1992**, *53*, 935–939.

[16] T. Chatterji, P. F. Henry, R. Mittal, S. L. Chaplot, *Phys. Rev. B* **2008**, *78*, 134105.

[17] E. E. Rodriguez, A. Llobet, T. Proffen, B. C. Melot, R. Seshadri, P. B. Littlewood, A. K. Cheetham, *J. Appl. Phys.* **2009**, *105*, 114901.

[18] B. K. Greve, K. L. Martin, P. L. Lee, P. J. Chupas, K. W. Chapman, A. P. Wilkinson, *J. Am. Chem. Soc.* **2010**, *132*, 15496–15498.

[19] Y. Kawamura, H. Mashiyama, K. Hasebe, *J. Phys. Soc. Japan* **2002**, *71*, 1694–1697.

[20] Y. Rakita, S. R. Cohen, N. K. Kedem, G. Hodes, D. Cahen, *MRS Commun.* **2015**, *5*, 623–629.

[21] I. Chung, J.-H. Song, J. Im, J. Androulakis, C. D. Malliakas, H. Li, A. J. Freeman, J. T. Kenney, M. G. Kanatzidis, *J. Am. Chem. Soc.* **2012**, *134*, 8579–8587.

[22] A. L. Goodwin, M. Calleja, M. J. Conterio, M. T. Dove, J. S. O. Evans, D. A. Keen, L. Peters, M. G. Tucker, *Science* **2008**, *319*, 794–7.

[23] O. J. Weber, B. Charles, M. T. Weller, *J. Mater. Chem. A* **2016**, *Advance Article*.

[24] A. C. Larson, R. B. Von Dreele, *General Structure Analysis System*; Technical Report no. 86-748; Los Alamos National Laboratory: Los Alamos, NM, **2000**.

[25] B. H. Toby, *J. Appl. Crystallogr.* **2001**, *34*, 210–213.

# COMMUNICATION

The hybrid perovskite formamidinium lead iodide undergoes two structural transitions in the 90 K to 490 K range. Unravelling these points to unusually large thermal expansion in the tetragonal phases, and strong coupling between the reentrant lower temperature structural transition and the optical band gap.

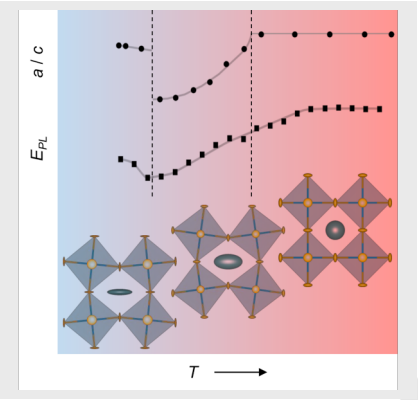


*D. H. Fabini, C. C. Stoumpos, G. Laurita, A. Kaltzoglou, A. G. Kontos, P. Falaras, M. G. Kanatzidis, R. Seshadri**

***Page No. – Page No.***

**Reentrant Structural and Optical Properties and Large Positive Thermal Expansion in Perovskite Formamidinium Lead Iodide**

## Atom Positions, $\alpha$-HC(NH$_2$)$_2$PbI$_3$ ($Pm\bar{3}m$, no. 221)

| Atom/Moiety | x | y | z | Wyckoff Site |
|---|---|---|---|---|
| $A$ | 0.5 | 0.5 | 0.5 | 1b |
| Pb | 0 | 0 | 0 | 1a |
| I | 0.5 | 0 | 0 | 3d |

## Atom Positions, $\beta$- and $\gamma$-HC(NH$_2$)$_2$PbI$_3$ ($P4/mbm$, no. 127)

| Atom/Moiety | x | y | z | Wyckoff Site |
|---|---|---|---|---|
| $A$ | 0.5 | 0 | 0.5 | 2c |
| Pb | 0 | 0 | 0 | 2a |
| I1 | 0 | 0 | 0.5 | 2b |
| I2 | $x$ | $x$+0.5 | 0 | 4g |

## Temperature-Dependent HC(NH$_2$)$_2$PbI$_3$ Crystal Structure Parameters

| $T$ (K) | Phase | Space Group | $a$ (Å) | $c$ (Å) | I2 $x$-coordinate |
|---|---|---|---|---|---|
| 489 | $\alpha$ | $Pm\bar{3}m$ | 6.402230(4) | - | - |
| 450 | $\alpha$ | $Pm\bar{3}m$ | 6.394969(4) | - | - |
| 399 | $\alpha$ | $Pm\bar{3}m$ | 6.384013(4) | - | - |
| 348 | $\alpha$ | $Pm\bar{3}m$ | 6.372556(4) | - | - |
| 299 | $\alpha$ | $Pm\bar{3}m$ | 6.357878(4) | - | - |
| 274 | $\beta$ | $P4/mbm$ | 8.971650(17) | 6.348355(24) | 0.26609(13) |
| 248 | $\beta$ | $P4/mbm$ | 8.956081(9) | 6.341941(11) | 0.27405(9) |
| 224 | $\beta$ | $P4/mbm$ | 8.937057(11) | 6.333945(12) | 0.27828(9) |
| 200 | $\beta$ | $P4/mbm$ | 8.922756(12) | 6.326256(14) | 0.28156(9) |
| 174 | $\beta$ | $P4/mbm$ | 8.907557(13) | 6.317806(14) | 0.28346(9) |
| 151 | $\beta$ | $P4/mbm$ | 8.895152(14) | 6.309463(16) | 0.28420(10) |
| 124 | $\gamma$ | $P4/mbm$ | 8.887796(22) | 6.288927(32) | 0.27631(15) |
| 101 | $\gamma$ | $P4/mbm$ | 8.875158(30) | 6.279170(40) | 0.27475(18) |
| 91 | $\gamma$ | $P4/mbm$ | 8.871316(29) | 6.276300(40) | 0.27453(17) |

## Bragg Peak Width Analysis

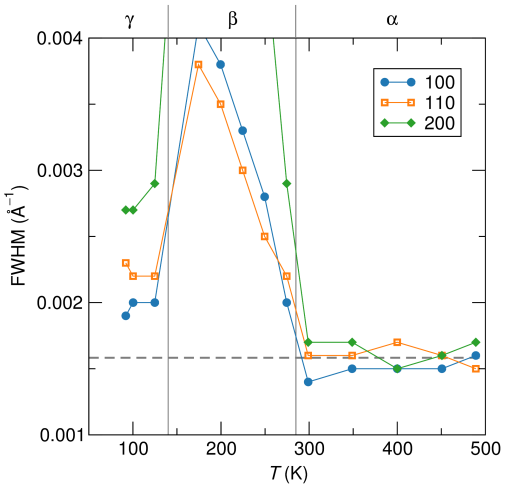


Figure S1: Full width at half maximum (FWHM) of low angle Bragg peaks that undergo tetragonal splitting, assuming a single, un-split peak. The onset of the continuous $\alpha$–$\beta$ transition is evident in the splitting of the $h00$ and $hk0$ peaks around ambient temperature. The peak widths in the $\gamma$-phase are indicative of multiple overlapping peaks, and are thus inconsistent with an alternative, truly cubic unit cell, such as that for the $a^+a^+a^+$ tilt system with $Im\bar{3}$ space group symmetry.

## Raw Photoluminescence Spectra

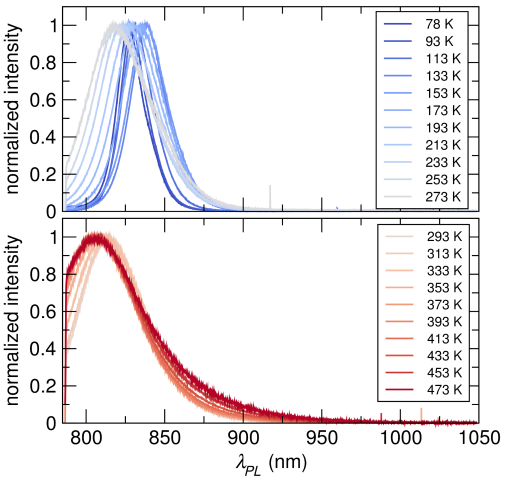


Figure S2: Variable temperature photoluminescence spectra below and above ambient temperature, normalized to peak emission intensity.

## Structure Solution Methodology

Phase transition temperatures and orders were determined by detailed analysis of Bragg peak emergence and splitting including the peak width analysis presented above, as well as comparison with reported scanning calorimetry [1]. The allowed "simple" octahedral tilting systems in perovskites that maintain 3-D corner connectivity have been enumerated [2], as well as those that allow displacement of the *B*-site cation [3], so a full structure solution from powder data is not necessary. Rather, these candidate structure models were screened for plausibility via whole pattern (Le Bail) fitting.

For the $\beta$-phase, the four tilt systems [2] that may be connected by a continuous phase transition to the cubic $Pm\bar{3}m$ aristotype ($a^0a^0a^0$ tilts) were screened, and the assignment of $P4/mbm$ symmetry ($a^0a^0c^+$ tilts) is unambiguous.

For the $\gamma$-phase, there is no constraint that the space group symmetry be related to that of the $\beta$-phase by any group-subgroup relation because the transition is first order. Accordingly, all 15 allowed simple tilt systems [2] were screened, as well as the 17 that combine *B*-site cation displacements with no tilts ($a^0a^0a^0$) or uniaxial tilts ($a^0a^0c^+$ or $a^0a^0c^-$) [3]. We assign the system with $a^0a^0c^+$ tilts and no *B*-site cation displacements (space group $P4/mbm$) based on the exact agreement between predicted and observed Bragg reflections and the goodness-of-fit in Rietveld refinement. Weak but somewhat "structured" diffuse scattering is observed at low temperatures that is not indexed by any plausible candidate crystallographic structure, indicating complex disorder or correlated motion of molecular cations. The pseudo-cubic cell causes substantial Bragg peak overlap, resulting in correlations between some refined structural parameters.

The most plausible alternative crystallographic models for the $\gamma$-phase are those of $a^+a^+a^+$ tilts (space group $Im\bar{3}$), $a^0b^+b^+$ tilts (space group $I4/mmm$), and $a^+b^+c^+$ tilts (space group $Immm$), which exhibit similar Bragg reflections in powder diffraction. These alternatives are rejected based on the absence of any detectable scattering intensity for certain expected low angle Bragg peaks and both poorer fitting and stronger parameter correlations in Rietveld refinement. Additionally, the Bragg peak width analysis above shows the data are incompatible with the truly cubic $a^+a^+a^+$ tilt system ($Im\bar{3}$).

The Bragg reflections from the structure that exhibits *B*-site cation displacements along the cubic [001] direction as well as $a^0a^0c^+$ tilts (space group $P4bm$) are indistinguishable from those of the $a^0a^0c^+$ tilt system with no *B* displacements ($P4/mbm$) when the cell is pseudo-cubic. We reject this alternative model in favor of its centrosymmetric parent because there is no evidence for such displacements, as in artificially elevated Pb atomic displacement parameters when refined in a high symmetry environment. Though there is a tendency for lone pair stereochemical activity in these main-group halides that would cause Pb displacements, this behavior is suppressed by the octahedral tilting present in the low temperature phases [4].

## References


1. D. H. Fabini, T. Hogan, H. A. Evans, C. C. Stoumpos, M. G. Kanatzidis, R. Seshadri, *J. Phys. Chem. Lett.* **2016**, *7*, 376–381.
2. C. J. Howard, H. T. Stokes, *Acta Crystallogr. Sect. B Struct. Sci.* **1998**, *54*, 782–789.
3. H. T. Stokes, E. H. Kisi, D. M. Hatch, C. J. Howard, *Acta Crystallogr. Sect. B Struct. Sci.* **2002**, *58*, 934–938.
4. D. H. Fabini, G. Laurita, J. S. Bechtel, C. C. Stoumpos, H. A. Evans, A. G. Kontos, Y. S. Raptis, P. Falaras, A. Van der Ven, M. G. Kanatzidis, R. Seshadri, *J. Am. Chem. Soc.* **2016**, *138*, 11820–11832.